

# Ultra-high-contrast few-cycle pulses for multipetawatt-class laser technology

Julia M. Mikhailova,<sup>1,2,\*</sup> Alexander Buck,<sup>1,3</sup> Antonin Borot,<sup>4</sup> Karl Schmid,<sup>1</sup> Christopher Sears,<sup>1</sup> George D. Tsakiris,<sup>1</sup> Ferenc Krausz,<sup>1,3</sup> and Laszlo Veisz<sup>1,5</sup>

<sup>1</sup>Max-Planck-Institut für Quantenoptik, Hans-Kopfermann-Strasse 1, 85748 Garching, Germany

<sup>2</sup>A. M. Prokhorov General Physics Institute, Russian Academy of Sciences, 38 Vavilov Street, 119991 Moscow, Russia

<sup>3</sup>Department für Physik, Ludwig-Maximilians-Universität, Am Coulombwall 1, 85748 Garching, Germany

<sup>4</sup>Laboratoire d'Optique Appliquée, Ecole Polytechnique, CNRS, F-91761 Palaiseau, France

<sup>5</sup>e-mail: laszlo.veisz@mpq.mpg.de

\*Corresponding author: julia.mikhailova@mpq.mpg.de

Received June 13, 2011; accepted June 26, 2011;

posted July 18, 2011 (Doc. ID 148952); published August 10, 2011

We report the generation of few-cycle multiterawatt light pulses with a temporal contrast of  $10^{10}$ , when measured as close as 2 ps to the pulse's peak. Tens of picoseconds before the main pulse, the contrast value is expected to spread much beyond the measurement limit. Separate measurements of contrast improvement factors at different stages of the laser system indicate that real contrast values may reach  $10^{19}$  and  $10^{14}$ , when measured 50 and 25 ps before the pulse's peak, respectively. The combination of the shortest pulse duration and the highest contrast renders our system a promising front-end architecture for future multipetawatt laser facilities. © 2011 Optical Society of America

OCIS codes: 320.7090, 190.4970, 140.7090.

Optical fields of relativistic intensities turn matter into hot, fully ionized plasma whose electrons acquire velocities approaching the speed of light [1]. Thanks to high-power lasers, these unique physical conditions can now be realized in small-scale laboratories and constitute the main subject of relativistic optical science [1]. Many areas of this science benefit from a combination of few-cycle duration with ultrahigh temporal contrast of powerful laser pulses. The few-cycle duration is crucial for the generation of intense isolated attosecond pulses in the relativistic laser–solid interaction [2] and helpful in particle acceleration [3]. Moreover, in combination with pulse energies of  $\sim 100$  mJ–100 J, the few-cycle pulse duration allows for reaching peak powers of  $\sim 10$  TW–10 PW from systems with unparalleled compactness. At relativistic intensities, the temporal contrast, defined as the ratio of the pulse's peak intensity to the intensity at a given time instant before the peak, is critical for a well-controlled laser–matter interaction experiment. Premature ionization of matter by the pulse-preceding background, typically consisting of prepulses, nano or picosecond pedestals, and a nonexponential leading edge of the main pulse, results in the formation of a rapidly expanding plasma long before the arrival of the main pulse. This effect radically modifies target conditions and seriously limits experiments that rely on the interaction of light with solid-density plasmas.

To the best of our knowledge, the highest previously achieved contrast value is  $\sim 10^{10}$  tens of picoseconds before the main pulse (with a duration of tens of femtoseconds) obtained by using either a cross-polarized wave generation (XPW) technique [4,5] or a plasma mirror (PM) [6]. Here we show that the integration of both techniques into the optical parametric chirped pulse amplification (OPCPA) system furnishes *few-cycle* multiterawatt light pulses with an intensity contrast of  $\sim 10^{10}$  when measured only 2 ps before the pulse peak. On a longer time scale, the contrast value exceeds our measurement limit but can be

estimated on the basis of separate measurements of contrast enhancement factors of XPW, OPCPA, and PM. The estimated contrast yields  $10^{19}$  and  $10^{14}$ , when measured 50 and 25 ps before the pulse peak, respectively. These estimations exceed previously reported state of the art by several orders of magnitude.

Our system is based on OPCPA [7] and is capable of generating pulses with a sub-three-optical-cycle duration (FWHM) and peak power of up to 16 TW [8]. The basic architecture of the system is shown in Fig. 1. In brief, 6 fs pulses at a central wavelength of 800 nm from a Ti:sapphire oscillator are amplified in a 1 kHz multipass Ti:sapphire amplifier and spectrally broadened in a neon-filled hollow core fiber (HCF). Temporally stretched by a negative-dispersion grism stretcher and acousto-optical modulator (Dazzler, FASTLITE) to the duration of 25 ps, these pulses provide a seed for two noncollinear OPCPA stages. The 532 nm pump pulses for OPCPA with a duration of 80 ps (FWHM) and energy of 1 J are optically synchronized with the seed pulses. Two OPCPA stages

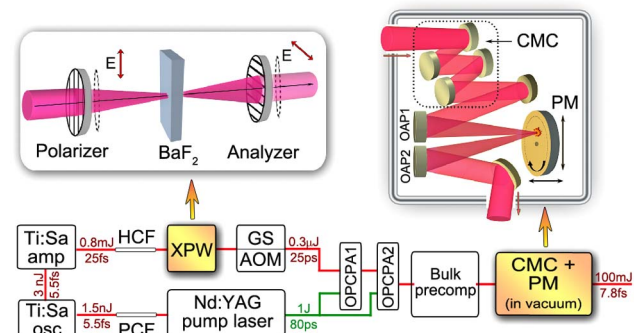


Fig. 1. (Color online) Schematic diagram of the system. PCF, photonic crystal fiber for optical synchronization of the pump and seed in OPCPA; GS, grism stretcher; AOM, acousto-optical modulator; CMC, chirped mirror compressor. The upper left panel shows the XPW scheme. The upper right panel shows the setup of the CMC and PM.

boost the seed pulse energy up to 170 mJ within the spectral band of 700–1000 nm, constituting a broadband parametric gain of more than  $10^5$ . After amplification, the chirped pulse is recompressed with a positive dispersion bulk glass precompressor and four chirped multilayer mirrors in a vacuum chamber.

The temporal contrast of the pulse is enhanced by virtue of short-pump OPCPA and two nonlinear-optical techniques highlighted in the upper panels of Fig. 1: XPW [4,5] and PM [9–11]. XPW is applied after the HCF, before OPCPA. To this end, the pulse is compressed by means of a double-angle chirped mirror compressor to a 6 fs duration and sent through a polarizer (upper left panel in Fig. 1) in order to enhance the purity of the linear polarization of the input beam. Next, it is focused into a 2 mm thick BaF<sub>2</sub> crystal, wherein the polarization of the short (thus intense) pulse is rotated in a third-order nonlinear process. The crossed polarizer after the crystal (the analyzer in Fig. 1) is used to suppress the residues of the original polarization. Finally, the beam is collimated and the “cleaned” pulse is stretched for seeding OPCPA. The conversion efficiency of XPW yields 15%. The cleaning technique based on a single PM (upper right panel in Fig. 1) is used at the final stage of the system after OPCPA and pulse recompression into the sub-10 fs regime. For this purpose, 130 mJ pulses are focused in the vacuum with an off-axis parabolic mirror (OAP) on an antireflection (AR)-coated glass target. Detrimental temporal pedestals, with the flux lower than the ionization threshold, are transmitted through an AR-coated target, while the main pulse is reflected from the plasma created on the target surface by the foot of the pulse. The light flux in the focus is  $\sim 10^4$  J/cm<sup>2</sup>. The AR-coated target is automatically rotated to provide a fresh surface for every laser shot. Regarding future applications, we note that our 6 in. diameter targets allow for the continuous operation of PM for more than 4 h at a 10 Hz repetition rate. The PM-reflected beam is collimated by a second OAP and sent to diagnostics of the reflected pulse energy, spectrum, duration, contrast, beam profile, and focus. The energy reflectivity of PM was measured to be  $\sim 80\%$ , resulting in 100 mJ output pulse energy. The pulse contrast was measured with a homebuilt high-dynamic-range third-order autocorrelator [12]. This instrument is based on third-harmonic generation (THG) in two consecutive beta barium borate (BBO) crystals and allows for measuring the intensity contrast over a dynamic range of about  $10^{10}$ .

The resultant THG autocorrelation trace of the pulse is shown by blue dots in Fig. 2. Here  $\tau_d$  denotes the time delay between the fundamental beam and sampling second harmonic in the THG process. The zero delay represents the peak of the pulse. The problematic pulse-preceding background is probed in the domain of negative delays. The inset of Fig. 2 shows the THG autocorrelation trace on a fine scale featuring the contrast value of  $10^9$  at  $\tau_d = -1.2$  ps. On a longer time scale, the real contrast is expected to exceed the dynamic range of our autocorrelator. To estimate its actual value, we measured the degree of contrast enhancement by each of the three cleaning techniques separately. The estimated contrast, calculated on the basis of measured contrast enhancement factors, is shown by the red (lower) line in Fig. 2. Below, we explain how this estimation was obtained.

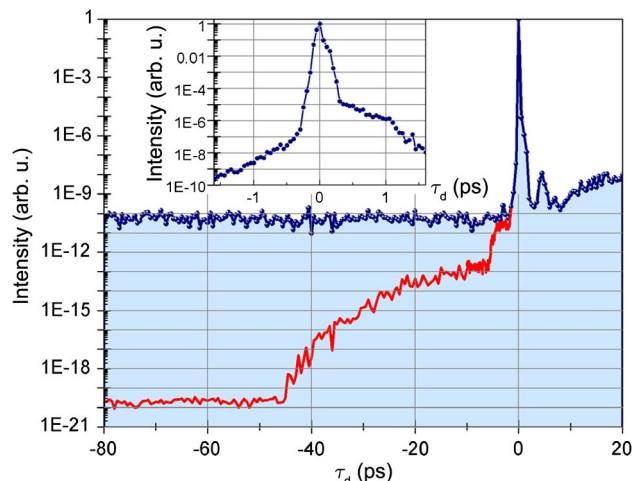


Fig. 2. (Color online) Resultant temporal contrast. Blue dots, measured THG autocorrelation with the dynamic range of about  $10^{10}$ . The actual contrast (red (lower) line) is estimated using measured contrast enhancement factors of OPCPA, XPW, and PM. The inset shows the measured THG autocorrelation on a fine scale.

The contrast enhancement by OPCPA is shown in Fig. 3(a), featuring THG autocorrelation traces before and after OPCPA stages. The seed pulse for OPCPA has a nanosecond pedestal with the contrast of  $C = 10^8$  at  $\tau_d = 80$  ps [gray (middle) line in Fig. 3(a)], which is due to amplified spontaneous emission in the Ti:sapphire amplifier. This pedestal is amplified by OPCPA only within a short duration of the OPCPA pump that is about 80 ps. The OPCPA energy gain is measured to be more than  $10^5$  ( $<1 \mu\text{J} \rightarrow 100 \text{ mJ}$ ) around the peak of the pump. Thus, outside the temporal window of the pump (i.e., for  $\tau_d < -45$  ps) the background is at least  $10^5$  times suppressed. In our measurements, the OPCPA gain was independent of the input contrast; therefore, to measure the contrast improvement due to OPCPA, we decreased the front-end contrast as is shown by the red (upper) line in Fig. 3(a). The contrast improvement is demonstrated by the fall of the autocorrelation from  $\tau_d \approx -10$  ps to  $\tau_d \approx -40$  ps, shown by the blue (lower) line in Fig. 3(a) as well as the green (upper) line in Fig. 3(b). The noise floor in Fig. 3(a) limits the observed contrast improvement to  $\sim 10^4$ , while the improvement of  $10^5$  is demonstrated by the green (upper) line in Fig. 3(b). The effect of the amplified parametric fluorescence (APF) creates an additional background within the OPCPA temporal window. In our measurements, it was not detected above the dynamic range of the correlator— $C \approx 2 \cdot 10^{10}$  at  $\tau_d = -10$  ps. Nevertheless, as a precaution we took the latter value into account as a lower limit of the APF contrast.

The contrast improvement by XPW is shown in Fig. 3(b). Here the green (upper) line depicts the THG autocorrelation measured with OPCPA only (XPW and PM bypassed) and the blue (middle) line shows the autocorrelation measured with XPW; both measurements were made with the decreased front-end contrast. An improvement of  $10^4$  due to XPW is clearly seen for  $\tau_d < -6$  ps. The contrast measured with XPW and OPCPA with optimal front-end contrast is shown by the gray (lower) line in Fig. 3(b). Note that the foot of the pulse extending over 5 ps  $< \tau_d < 100$  fs is not affected by XPW

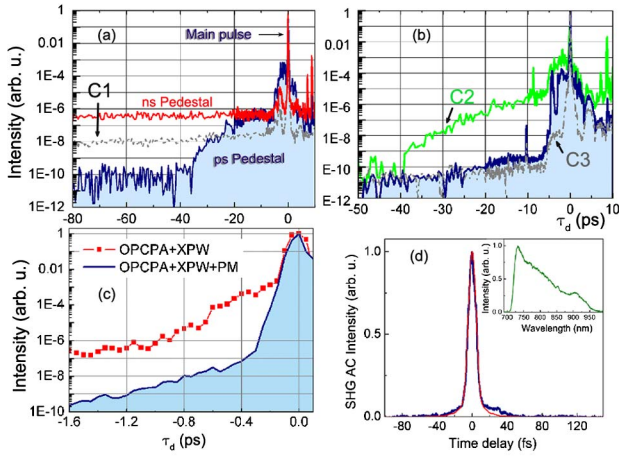


Fig. 3. (Color online) (a) THG autocorrelations taken before (red (upper) line) and after OPCPA (blue (lower) line). Gray (middle) line C1 shows a typical front-end contrast; red (upper) line, front-end contrast decreased for measuring the contrast enhancement. (b) THG autocorrelations measured at the output of the system without (green line C2) and with XPW (blue (middle) line) with a decreased front-end contrast. Gray line C3 shows the autocorrelation obtained with XPW with the optimal front-end contrast. (c) THG autocorrelations obtained without (red squares) and with PM (blue line). (d) Blue (upper) line, measured second-order autocorrelation after PM; red (lower) line, second-order autocorrelation, calculated from the laser spectrum (displayed in the inset) assuming constant phase.

because it originates from the stretching and compression of the few-cycle pulse after XPW.

The results of the contrast improvement by PM are shown in Fig. 3(c), where red squares show the THG autocorrelation when bypassing PM and the blue solid line denotes the result measured with PM. The contrast enhancement of 500 on average is clearly seen. This enhancement factor holds true for any delay  $\tau_d < -1.6$  ps because, as is seen from Fig. 3(c), the reflecting plasma starts to be generated at the surface of the AR-coated target at  $\tau_d \approx -0.3$  ps. Remarkably, even the foot of the pulse on a 100 fs scale is rendered steeper by PM. Measurements with a worse input contrast (bypassing XPW and/or with the misaligned front end) also demonstrated stable contrast improvement of  $\sim 500$  for delays  $\tau_d < -0.5$  ps. In fact, the improvement due to PM depends only on the reflectivity of the AR-coating of the PM target and the reflectivity of the generated plasma that was  $\sim 80\%$  independent of the input contrast in our operating conditions.

Based on measured contrast improvement factors of XPW, OPCPA, and PM and taking into account the lower limit of APF, one can estimate the real contrast as

$$C = \begin{cases} C1 \cdot 1/10^5_{(\text{OPCPA})} \cdot 1/10^4_{(\text{XPW})} \cdot 1/500_{(\text{PM})}, & \text{for } -80 \text{ ps} < \tau_d < -45 \text{ ps} \\ C2 / \max(C2)|_{\tau_d < -10 \text{ ps}} \cdot C1 \cdot 1/200_{(\text{XPW}+\text{APF})} \cdot 1/500_{(\text{PM})}, & \text{for } -45 \text{ ps} < \tau_d < -10 \text{ ps} \\ C3 \cdot 1/500_{(\text{PM})}, & \text{for } -10 \text{ ps} < \tau_d < -1.5 \text{ ps} \end{cases}$$

where the curves C1, C2, and C3 are denoted in Fig. 3 and C is shown by the red (lower) line in Fig. 2

The applicability of PM to few-cycle pulses required experimental verification, as PM could in principle alter the pulse duration by the effect of pulse chirping in expanding plasmas. We have measured, for the first time to our knowledge, the duration of the pulse before and after PM using a single-shot second-order autocorrelation [8]. The second-order autocorrelation taken after PM is shown by the blue dots in Fig. 3(d) and the red line shows the second-order autocorrelation calculated by Fourier transforming the pulse spectrum [shown in the inset of Fig. 3(d)], assuming the constant phase. The FWHM of the pulse envelope, deconvolved from the measured autocorrelation, is 7.8 fs and is not affected by PM.

The demonstrated ultrahigh-contrast few-cycle multi-terawatt light pulses open the door to a new class of high-field experiments, in which solid matter with sharp density gradients can be abruptly exposed to electromagnetic fields at relativistic intensities. Implications include the generation of isolated attosecond pulses at substantially increased photon energy and/or power levels. Moreover, this light source lends itself to further amplification in Ti:sapphire and/or OPCPA stages, offering a route to high-contrast multipetawatt pulses for exploring new physics [13].

This work is supported by the DFG-Project TR-18, by the Association EURATOM, Max-Planck-Institut für Plasmaphysik, and by the Munich Centre for Advanced Photonics (MAP) excellence cluster. J. M. Mikhailova acknowledges support from the Alexander-von-Humboldt Foundation and Russian Foundation for Basic Research (RFBR) grant 11-02-01217.

## References

1. G. Mourou, T. Tajima, and S. V. Bulanov, *Rev. Mod. Phys.* **78**, 309 (2006).
2. G. D. Tsakiris, K. Eidmann, J. Meyer-ter-Vehn, and F. Krausz, *New J. Phys.* **8**, 19 (2006).
3. K. Schmid, L. Veisz, F. Tavella, S. Benavides, R. Tautz, D. Herrmann, A. Buck, B. Hidding, A. Marcinkevicius, U. Schramm, M. Geissler, J. Meyer-ter-Vehn, D. Habs, and F. Krausz, *Phys. Rev. Lett.* **102**, 124801 (2009).
4. A. Jullien, O. Albert, F. Burgy, G. Hamoniaux, J.-P. Rousseau, J.-P. Chambaret, F. Augé-Rochereau, G. Chériaux, J. Etchepare, N. Minkovski, and S. M. Saitiel, *Opt. Lett.* **30**, 920 (2005).
5. V. Chvykov, P. Rousseau, S. Reed, G. Kalinchenko, and V. Yanovsky, *Opt. Lett.* **31**, 1456 (2006).
6. A. Levy, T. Ceccotti, P. D'Oliveira, F. Réau, M. Perdrix, F. Quéré, P. Monot, M. Bougeard, H. Lagadec, Ph. Martin, J.-P. Geindre, and P. Audebert, *Opt. Lett.* **32**, 310 (2007).
7. A. Dubietis, G. Jonušauskas, and A. Piskarskas, *Opt. Commun.* **88**, 437 (1992).
8. D. Herrmann, L. Veisz, R. Tautz, F. Tavella, K. Schmid, V. Pervak, and F. Krausz, *Opt. Lett.* **34**, 2459 (2009).
9. H. Kapteyn, M. Murnane, A. Szoke, and R. Falcone, *Opt. Lett.* **16**, 490 (1991).
10. B. Dromey, S. Kar, M. Zepf, and P. Foster, *Rev. Sci. Instrum.* **75**, 645 (2004).
11. G. Doumy, F. Quere, O. Gobert, M. Perdrix, Ph. Martin, P. Audebert, J. C. Gauthier, J.-P. Geindre, and T. Wittmann, *Phys. Rev. E* **69**, 026402 (2004).
12. F. Tavella, K. Schmid, N. Ishii, A. Marcinkevicius, L. Veisz, and F. Krausz, *Appl. Phys. B* **81**, 753 (2005).
13. <http://www.extreme-light-infrastructure.eu/>.